BILINGUAL PUBLISHING GROUP

Journal of Atmospheric Science Research

https://journals.bilpubgroup.com/index.php/jasr/index

ARTICLE

Kelvin Wave Propagation over a Sloping Interface and Relationships with El Niño Southern Oscillation

***Gian Luca Eusebi Borzelli*[1*], *Arnold Sullivan*[2,3]**

[1] *Center for Remote Sensing of the Earth (CERSE), Rome, 00153, Italy*

[2] *CSIRO, Environment, Aspendale, 3195, Australia*

[3] *School of Earth, Atmosphere, and Environment, Monash University, Melbourne, 3800, Australia*

ABSTRACT

Internal Kelvin Wave (KW) propagation is studied about variations in the sea surface temperature anomaly (SSTA) over the tropical Pacific. Temperature and Salinity (TS) observations have been used to define the vertical structure of the ocean about the propagation properties of KWs. Changes in the vertical structure of the water column determine consistent zonal variations in the wave velocity, with values varying, roughly, from 1.8 to 2.6 m/s. The authors document that KWs are formed regularly at the western boundary of the tropical Pacific, but, in these cases, never overcome the dateline. Occasionally, KWs are generated in the region comprised between 170°E and 170°W, and, on all these occasions, a positive phase of the El Niño Southern Oscillation (El Niño) event is recorded. A model, named Sloping Interface Model (SIM), is proposed to relate changes in the pycnocline depth, associated with transiting KWs, and SST anomaly variations. In the SIM, whose equations are consistent with the Recharge/Discharge paradigm, the ocean is described as a two-layer system and the climatological state, represented by a sloping pycnocline, is maintained by a constant easterly wind stress. Using the SIM and coherently with the Recharge/Discharge paradigm, the authors show that changes in the averaged SSTA over El Niño 3, 3.4 and 4 regions are nearly perfectly correlated to pycnocline displacements due to transiting KWs.

***Keywords*:** Kelvin Wave propagation; Pycnocline depth; Sea surface temperature; El Niño Southern Oscillation (ENSO)

*CORRESPONDING AUTHOR:

Gian Luca Eusebi Borzelli, Center for Remote Sensing of the Earth (CERSE), Rome, 00153, Italy; Email: luca_borzelli@yahoo.it

ARTICLE INFO

Received: 27 January 2024 | Revised: 11 March 2024 | Accepted: 15 March 2024 | Published Online: 26 March 2024

DOI: https://doi.org/10.30564/jasr.v7i2.6228

CITATION

Borzelli, G.L.E., Sullivan, A., 2024. Kelvin Wave Propagation over a Sloping Interface and Relationships with El Niño Southern Oscillation. Journal of Atmospheric Science Research. 7(2): 1–18. DOI: https://doi.org/10.30564/jasr.v7i2.6228

1. Introduction

In the Tropical Pacific, the most intriguing and widely studied climatic oscillation is El Niño Southern Oscillation (ENSO). The ENSO cycle is the result of an ocean-atmosphere feedback [1,2], which produces an irregular oscillation between a warm (El Niño) and a cold (La Niña) phase, peaking in boreal winter and recurring every 2–5 years [3–5]. During its cold phase, intensified trade winds accumulate warm water into the west, causing the thermocline to deepen and develop a large zonal slope. During its warm phase, westerly winds advect warm waters eastward and cause the zonal structure of the thermocline to become more horizontal. Over the last few decades, numerous studies have been conducted to understand the dynamics underlying the ENSO cycle. Most of these studies dealt with the oscillatory nature of the phenomenon and focused on the coupling between changes in the depth of the main thermocline, heat content in the surface layer of the water column, and oceanic feedback on the zonal wind pattern. These theories can be grouped into two main categories: in the first, ENSO is regarded as a nearly self-sustained oscillation determined by heat accumulation (recharge) and discharge in the equatorial Pacific. In these theories, the subsurface memory of the ocean (i.e., the heat stored in the surface layer), depends on the depth of the thermocline, and the zonal shape of the isothermal surfaces is sustained by the dynamical balance between the zonal pressure gradient and the trade winds [2,6]. This process systematically transfers heat westward and "charges" the western part of the basin, which is then "discharged" through eastward energy redistribution associated with the collective action of internal oceanic waves. This interpretation, which explicitly filters out fast propagation processes to emphasize the collective effect of tropical internal oceanic waves, leads to regard ENSO as a quasi-steady zonal oscillation of the tropical Pacific [7,8]. It is consistent with the long-lead predictability of ENSO [9,10], but it only marginally explains the irregularity and different behaviors of different ENSO episodes.

In the second approach, although conceptually similar to the Recharge/Discharge about the importance of subsurface adjustment processes, ENSO is viewed as a damped oscillation that is explicitly triggered by freely propagating equatorial waves, generated by the wind and/or reflected by the western Pacific boundary [11,12]. According to this model, the delayed negative feedback resulting from the generation, propagation, and reflection of equatorial oceanic waves at the western Pacific boundary is responsible for the phase reversal of the ENSO cycle.

The approaches described above are descriptive and prognostic tools, which are useful for describing the initiation and evolution of El Niño. However, they are difficult to relate to the fundamental equations and processes that govern the fluid dynamics associated with El Niño. In their study, Picaut and Delcroix [13] focused on the 1986–1987 El Niño and 1988–1989 La Niña events and demonstrated that El Niño initiation was characterized by the occurrence of Kelvin (KWs) and Rossby waves (RWs) that were excited by a series of westerly wind events (WWEs) in the central tropical Pacific. Fedorov et al. [14] analyzed the predictability of ENSO in relation to atmospheric disturbances such as WWEs. Arora [15] and Arora and Kuman [16] used an Ocean General Circulation Model (OGCM) to study the impact of wind variability on ENSO. These studies all highlight the significant role of WWEs in triggering El Niño through the excitation of KWs and RWs (see also Wang and Fiedler [17] and Santoso et al. [18]). However, despite this evidence, Kang and An [19] observed that the contributions of KWs and RWs to changes in the SST cancel each other out over a flat pycnoline, as it is in the western equatorial Pacific, while in the eastern part of the basin, where the pycnocline is sloping, SST variations are primarily driven by KWs. In a recent study, Eusebi Borzelli and Carniel [20] examined the convergence of easterly and westerly winds and its impact on El Niño initiation. They found that when the wind convergence shifts east of 175°E, an El Niño event is triggered. The authors attributed this to the fact that in the tropical Pacific, the main pycnocline starts sloping east of 175°E. When the pycnoclyne is sloping, KWs and RWs propagate

differently: Since KWs are constrained to propagate along the zonal direction, to conserve energy and potential vorticity when propagating over a lowering pycnocline, they shrink meridionally and increase their amplitude [21]. Conversely, the flow associated with RWs is not constrained zonally and when propagating over a lowering pycnocline, to conserve energy and potential vorticity, RWs deviate poleward, leave the region around the equator [21] and no longer interact with KWs that are left to modify efficiently the depth of the thermocline.

This research aims to explore the relationships between KW propagation and changes in the SSTA, with a specific focus on El Niño initiation. By using Absolute Dynamic Topography (ADT) data provided by orbiting altimeters, we show that internal KWs are formed regularly along the western boundary of the Pacific Ocean and occasionally in the central Pacific (i.e., between 170°E and 170°W), but, predominantly, only KWs formed in the central Pacific contribute to El Niño initiation and variability.

Additionally, we show that the anomaly in the KW amplitude (i.e., KW activity) averaged over El Niño 3 (5°S–5°N, 150°W–90°W), 4 (5°S–5°N, 160°E–150°W) and 3.4 (5°S–5°N, 170°W–120°W) regions is closely related to the SSTA averaged over the same regions, with an RMS error between the two data sets on the order of 10%. To explain this relationship, we developed an analytical model, referred to as the SIM (see Appendix for details). This model is based on fundamental hydrodynamic equations and connects changes in the spatially averaged SSTA in regions symmetric with respect to the equator, to the variability in the KW activity anomaly. In the SIM, which is essentially a propagation model for internal KWs over a sloping interface, the Pacific Ocean is described as a two-layer system and the climatological state, represented by the sloping pycncoline, is maintained by a constant easterly wind stress. The sloping interface determines the damping of the propagating KW. The SIM equations are consistent and equivalent to the prognostic equations of the Recharge/Discharge model developed by Jin [7,8] and Burger and Jin [22], but with the difference that, in the SIM, coefficients are associated with specific oceanic parameters.

2. Materials and methods

Weekly, in situ Temperature-Salinity (TS) data sampled on a regular spatial grid of 0.25° × 0.25°, over 50 vertical levels (from 0 to 5500 m), covering the region 15°S–15°N 130°E–80°W in the period 6 Jan 1993–25 Dec 2019, were provided by the Copernicus Marine Environment Monitoring Service of the European Union. The Copernicus data was used to compute seawater density profiles ($\rho(x,y,z,t)$) for each point in the observation area and each date during the observation period.

The ocean was represented as a two-layer system, with the depth of each layer determined by fitting density profiles with a step function using a least-square method. This involved dividing the water column into two segments at each point in the observation domain and calculating average densities for each segment. The resulting two-layer representations were compared to the original density profile, and the one with the lowest root-mean-square was selected as the best two-layer representation of the water column vertical structure. The internal wave velocity was computed from the two-layer representation of the ocean using the formula $c_1(x,y,t) = [g'(x,y,t) \cdot H_1(x,y,t)]^{1/2}$, where H_1 is the depth of the surface layer (i.e., the pycnocline depth) and g' is the reduced gravity (i.e., $g' = g \cdot (\rho_2 - \rho_1)/\rho_2$ with ρ_1 and ρ_2 the densities of the surface and bottom layer, respectively).

The damping coefficient, $\gamma = [\tau_x/(D_1\rho_1)]$, discussed in Appendix, was computed by fitting a straight line to the mean depth of the pycnocline between 5°S and 5°N, averaged over the entire observation period, and observing that the slope of the equilibrium interface layer is $\partial h_{eq}/\partial x = -\tau_x/(g' D_1 \rho_2) = -(\gamma/g') \cdot (\rho_1/\rho_2)$ (note that τ_x is negative because represents easterly winds). D_1 (≈ 147 m) was set as the mean depth of the pycnocline between 5°S–5°N, 130°E–80°W averaged over the entire observation period.

Daily ADT data with spatial resolution of 0.25° ×

0.25° provided by orbiting altimeters and processed by Copernicus were re-sampled over the same temporal grid of TS observations using a cubic spline. Following Boulanger and Menkes [23,24] and Boulanger et al. [25], KW amplitudes were computed by expressing the ADT (η) as a linear superposition of freely propagating Rossby and Kelvin waves, namely,

$$\eta(x,y,t) = \sum_{n=0}^{\infty} r_n(x,t) \cdot R_n\left(\sqrt{\frac{\beta}{2c}}y\right)$$

where r_0 is the KW amplitude and R_n (n = 1,2...) are functions related to the parabolic cylinder functions (for details on the derivation, see relevant references [23,26]). Here, c (≈ 2.2 m/s) was set as the mean of $c_1(x,y,t)$ over the region (5°S–5°N, 130°E–80°W), averaged over the entire observation period. Note that, using this approach, r_0 is actually the KW amplitude and no further filtering is necessary to capture the variability in the sea surface structure associated with propagating KW.

The SST anomaly (SSTA) was estimated using the HadISST data set. SSTA and KW amplitude anomaly (i.e. the anomaly, $\sigma_0(x,t)$, of r_0 re-sampled every month) were computed by taking as the baseline climatology the period Jan 1993–Dec 2019. Then, we computed the mean spatial values of the SSTA and KWs activity (KWA, quantified as $\sigma_0(x,t) \cdot R_0(y \cdot (\beta/2c_1)^{1/2})$) over the El Niño 3 (5°S–5°N, 150°W–90°W), 4 (5°N–5°S, 160°E–150°W) and 3.4 (5°S–5°N, 170°W–120°W) regions.

3. Results

Figures 1a and 1b show the average depth of the pycnocline over the observation period and the mean surface density anomaly (i.e., σ_t = density – 1000 kg/m^3) distribution, respectively. The density anomaly of the bottom layer is not shown, because it remains substantially constant over the entire observation period and the entire Pacific, with an average value of σ_t = 27.27 kg/m^3 and a standard deviation of 0.05 kg/m^3. **Figures 1c and 1d** depict the standard deviations of the means shown in **Figures 1a and 1b**, respectively. Except for the region off the American coast, the pycnocline depth values are approximately 150 m throughout the equatorial Pacific, with an uncertainty given by a standard deviation of 20 m. Surprisingly, as we approach the American coast, the pycnocline depth increases. According to the available literature, the pycnocline depth is minimum near by the American coast [27]. To explain this apparent contradiction, it must be noted that the common practice for computing the pycnocline depth is the "Maximum Vertical Gradient" method, which determines the depth of the pycnocline as the depth at which the vertical gradient of the density is at its maximum. In this research, to use the theory of internal KW, we assumed that the ocean can be described as a two-layer system and therefore estimated the depth of the pycnocline by fitting vertical density profiles to a step function. While these two methods are equivalent in a strictly two-layer ocean, the fitting technique may produce unstable results when the vertical structure of the ocean becomes more complex. The region off the American coast is characterized by an offshore current originating from the Peruvian current, which consists of waters floating over superficial tropical Pacific waters. This results in a more complex vertical structure of the ocean compared to the rest of the tropical Pacific. In this region, the vertical structure of the ocean cannot be approximated by a two-layer system, making the results obtained with the step function fitting method quite unstable. Therefore, the high values of the pycnocline depth off the American coast are not in contrast with the data presented in the available literature. When comparing **Figures 1a and 1c**, it can be seen that the pycnocline depth values throughout the equatorial Pacific are approximately 150 m, with an uncertainty given by a standard deviation of 20 m. However, in the region off the American coast, the pycnocline depth appears to be 200 m, but with an uncertainty of 100 m.

Figures 2a and 2b show the spatial distribution of the first baroclinic mode velocity (c_1) averaged in the period 1993–2019 and its standard deviation, as deduced from density and pycnocline depth data shown in **Figure 1**. Surprisingly, the density of the

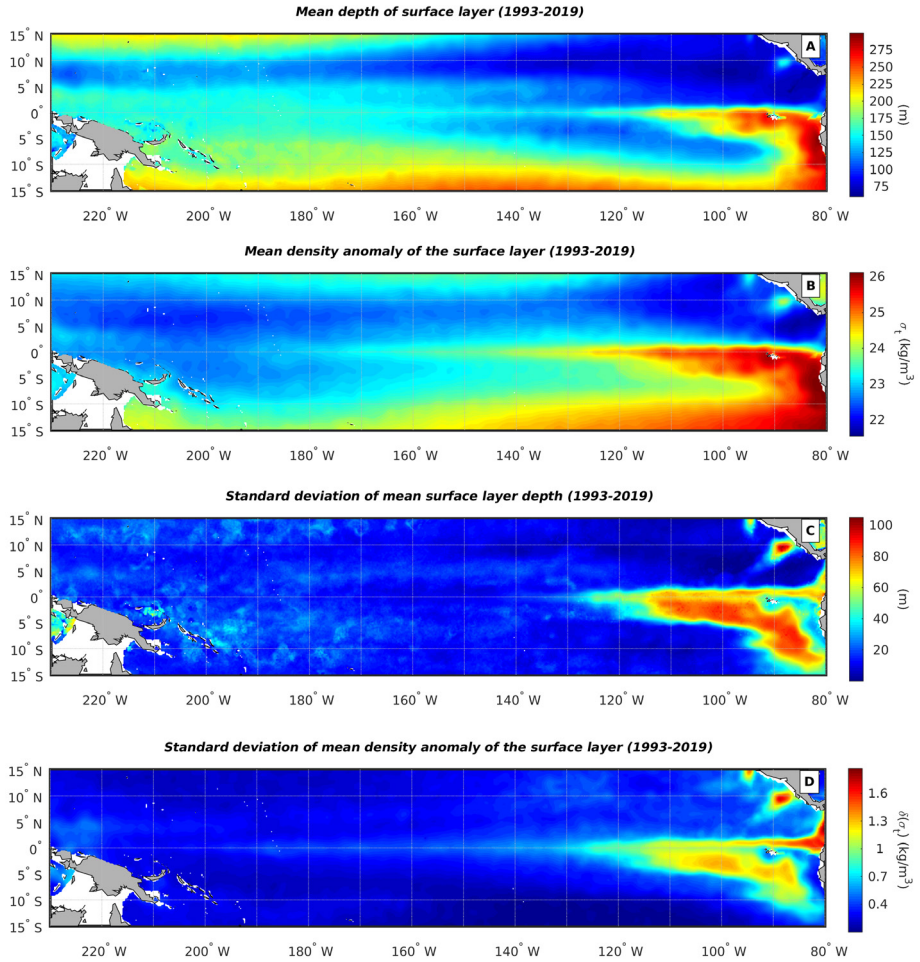

Figure 1. The mean depth of the pycncoline (**a**) and mean density anomaly of the surface layer (**b**) over the observation period. The standard deviation of the mean pycncoline depth (**c**) and standard deviation of the mean density anomaly of the surface layer (**d**).

surface layer and the depth of the pycnocline combine to determine remarkable zonal variations in the volocity of the first baroclinic mode (**Figure 2a**). These variations are asymmetric with respect to the equator and characterized by a southeast-northwest front, separating high values (≥ 2.3 m/s) in the west, from low values (≤ 2 m/s) in the east. Overall, **Figure 2b** shows values of the standard deviation, comprised between 0.15 m/s and 0.25 m/s, indicating that the temporal variability of the first baroclinic mode velocity is quite low (≈ 10%). It is interesting to note that, off the Peruvian coast, the high variability in the density of the surface layer and the pycncoline depth, compensate with each other determining a "nearly" stationary velocity field of the first baroclinic mode.

Figures 3a and 3b show the zonal variation between 130°E and 110°W (i.e., this region has been chosen to avoid the high variability region in the depth of the pycnocline in the easternmost part of the equatorial Pacific) in the meridional mean between 5°S and 5°N of the time averaged depth of the pycnocline and the time averaged density, respectively. In **Figure 3a**, the dashed, sloping line represents the linear fitting of the depth of the pycnocline. Note that the slope of this line is associated, according to what is discussed in Appendix, with the average wind stress through the formula $m = -\tau_x/(g'D_1\rho_2)$, which gives, with $m = 2.8\cdot10^{-6}$, $D_1 \approx 145$ m, $\rho_1 \approx 1023$ kg/m^3 and $\rho_2 \approx 1027$ kg/m^3, $\tau_x \approx 0.016$ N/m^2, which is equivalent to an average zonal wind velocity on the order of 3.2 m/s. Furthermore, note that the wave damping coefficient due to the sloping pycnocline is given, as discussed in Appendix, by $\tau_x/(2c_1^2D_1\rho_1) \approx 1.1\cdot10^{-8}$ m^{-1}, which implies a "damping distance" of the order of $9\cdot10^4$ km.

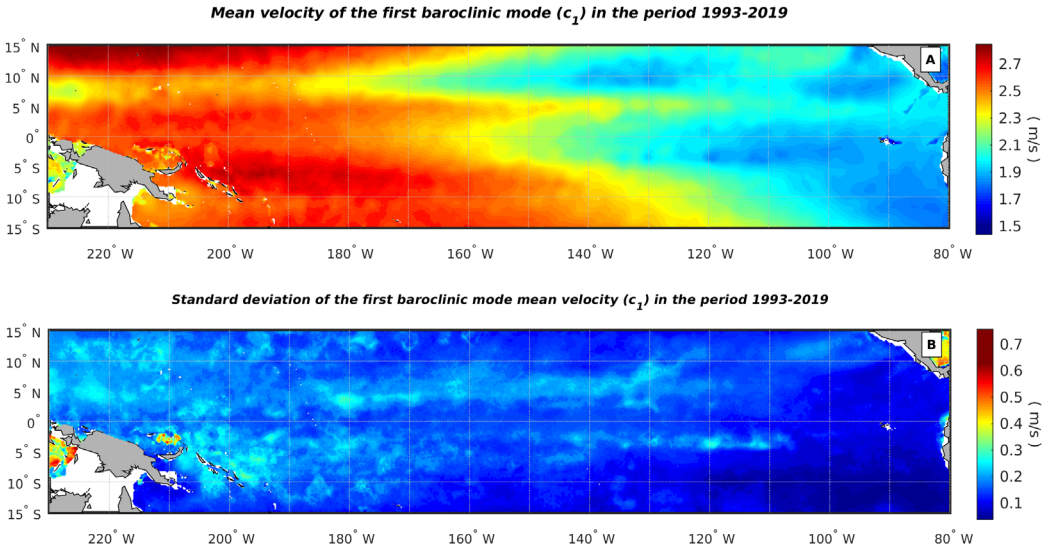

Figure 2. The mean velocity of the first baroclinic mode (c_1) over the observation period (**a**); standard deviation of the mean velocity of the first baroclinic mode (**b**).

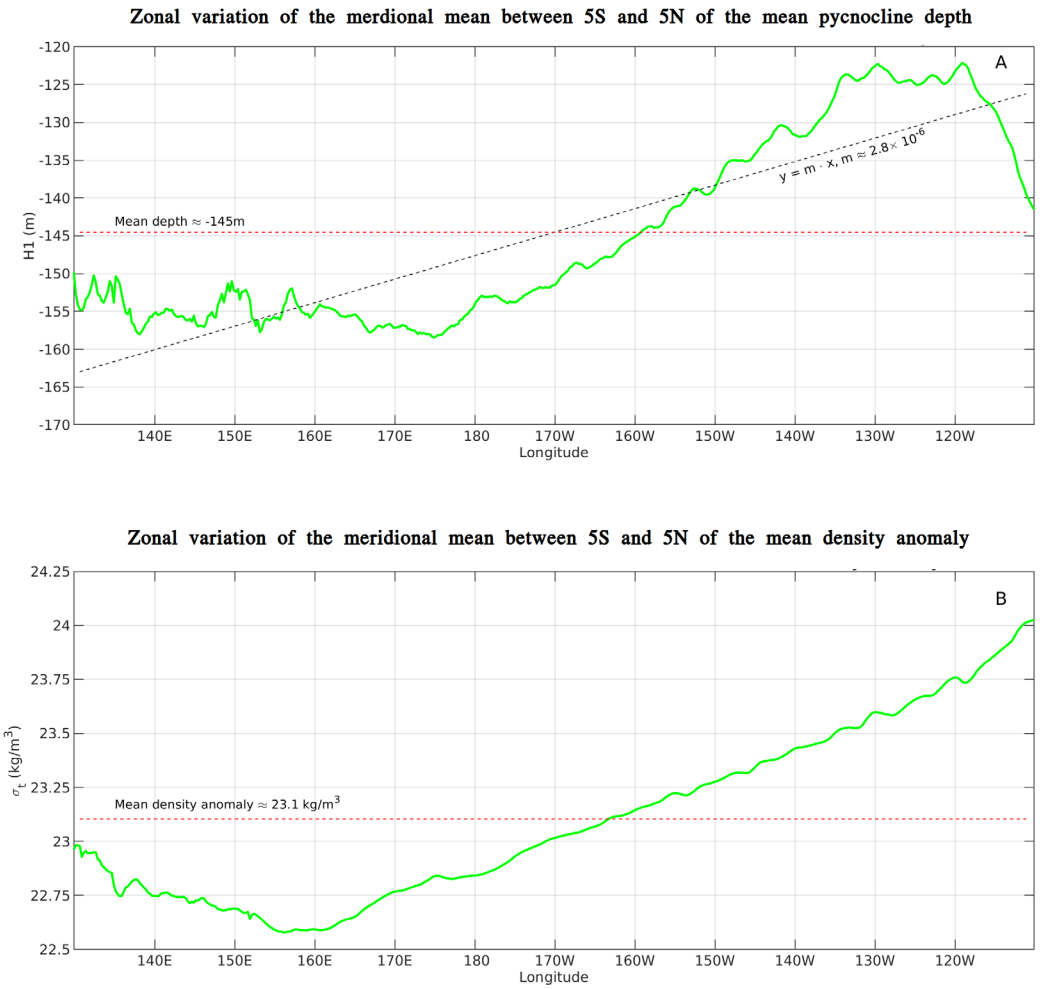

Figure 3. (**a**) Zonal variation in the meridional mean between 5°S and 5°N of the mean pycncoline depth; dashed black line represents the regression line of the, red dashed line represents the average depth of the pycncoline. (**b**) Zonal variation in the meridional mean between 5°S and 5°N of the mean surface density anomaly; red dashed line represents the average density anomaly of the surface layer.

Figure 4 shows the longitude-time plot of KWs amplitude. From the analysis of this figure, it is clear that, along the western Pacific coast KWs, which are possibly the result of the reflection by the western Pacific boundary to impinging Rossby Waves [24,25], are rather regularly excited every year, but never overcome the dateline. Conversely, during El Niño episodes (1994–1995, 1997–1998, 2002–2003, 2004–2005, 2006–2007, 2009–2010, 2014–2015, 2015–2016, 2018–2019 see colored bullets annotated on the left vertical axis of the figure), KWs originate near by the dateline (approximately between 170°E and 170°W) and reach the eastern Pacific boundary; during intense ENSO episodes (1998, 2016), KWs originate at 170°W and intrude definitely the eastern Pacific, reaching the eastern boundary of the basin. This circumstance confirms the observations of Boulanger and Mekens [24] and Eusebi Borzelli and Carniel [20], who found that the KW variability at periods longer than 6 months, which play an important role in El Niño onset, could be associated with wind variability in the vicinity of the dateline.

A different situation emerges when analyzing KWs amplitude in relation to La Niña episodes (1995–1996, 1998–1999, 1999–2000, 2000–2001, 2005–2006, 2007–2008, 2008–2009, 2010–2011, 2011–2012, 2016–2017, 2017–2018, as shown by the colored squares on the right vertical axis of **Figure 4**). During each La Niña episode, a clear pattern of low values can be observed emerging from the western Pacific coast, traveling freely through the tropical Pacific Ocean, and reaching the eastern boundary of the basin. This observation suggests an asymmetric behavior of El Niño/La Niña in relation to KWs propagation.

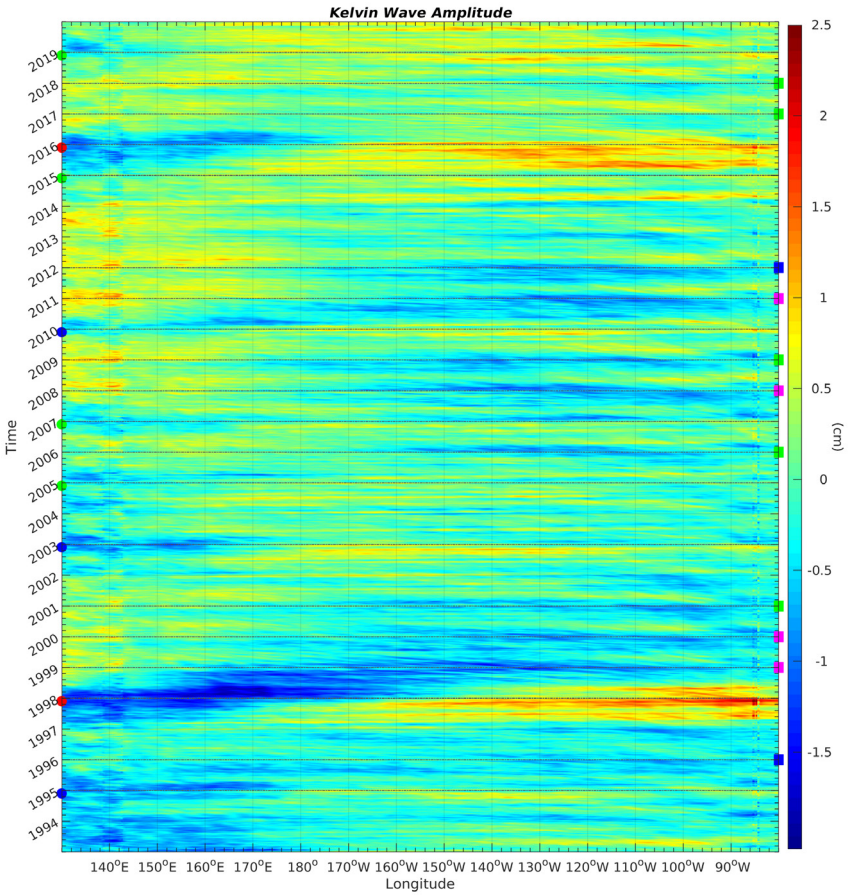

Figure 4. The longitude-time plot of KWs amplitude. Colored bullets on the left vertical axis of the picture, indicate El Niño years, the intensity of the event classified as follows: Green-weak event, blue-moderate event, magenta-strong event (in the examined period there were no strong events), red-Very strong event. Colored squares on the right vertical axis indicate La Niña years, with intensity of the event classified as follows: green-Weak event, blue-Moderate event, magenta-Strong event (see https://ggweather.com/enso/oni.htm for the classification scheme adopted).

Figure 5 depicts the SSTA over El Niño 3, 3.4 and 4 regions and the average over the same regions of the Kelvin Wave Activity (KWA) anomaly. Here, with KWA it is intended the quantity $r_0(x,t) \cdot exp[-(\beta/2c_1)\cdot y^2]$. In El Niño regions 3 (**Figure 5a**) and 3.4 (**Figure 5b**), the relation between SSTA and an average of the KWA anomaly is "nearly perfect", while it drops in region 4. This indicates that while in El Niño regions 3 and 3.4, variability in the averaged SSTA and average changes in the pycnocline depth associated with transiting KWs (denoted with Δ) are nearly perfectly in equilibrium (with reference to Appendix, in these regions we have $\partial\Delta/\partial t \approx 0$), in El Niño region 4, the equilibrium between the averaged SSTA and the average displacement of the pycnocline associated with transiting KWs, requires, to be achieved, to account for differences in the vertical displacement of the pycnocline at the zonal borders of the region (with reference to Appendix, this implies that, in this region, $\partial\Delta/\partial t \neq 0$).

Figure 6 depicts the SSTA (as in **Figure 5**, reported for the convenience of the reader) and $\partial\Delta/\partial t+\Delta$. Again, in El Niño regions 3 (**Figure 6a**) and 3.4 (**Figure 6b**), the relationship between SST and $\partial\Delta/\partial t+\Delta$ is "nearly" perfect and the contribution to the variability in the SSTA of the term $\partial\Delta/\partial t$ is negligible. In El Niño region 4, however, adding the term $\partial\Delta/\partial t$ to Δ, clearly improves the correlation between SSTA and the average vertical pycnocline displacement associated with transiting KWs, indicating that differences in the amplitude of incoming and outgoing waves at the zonal borders of the region are important to determine the variability in the SSTA.

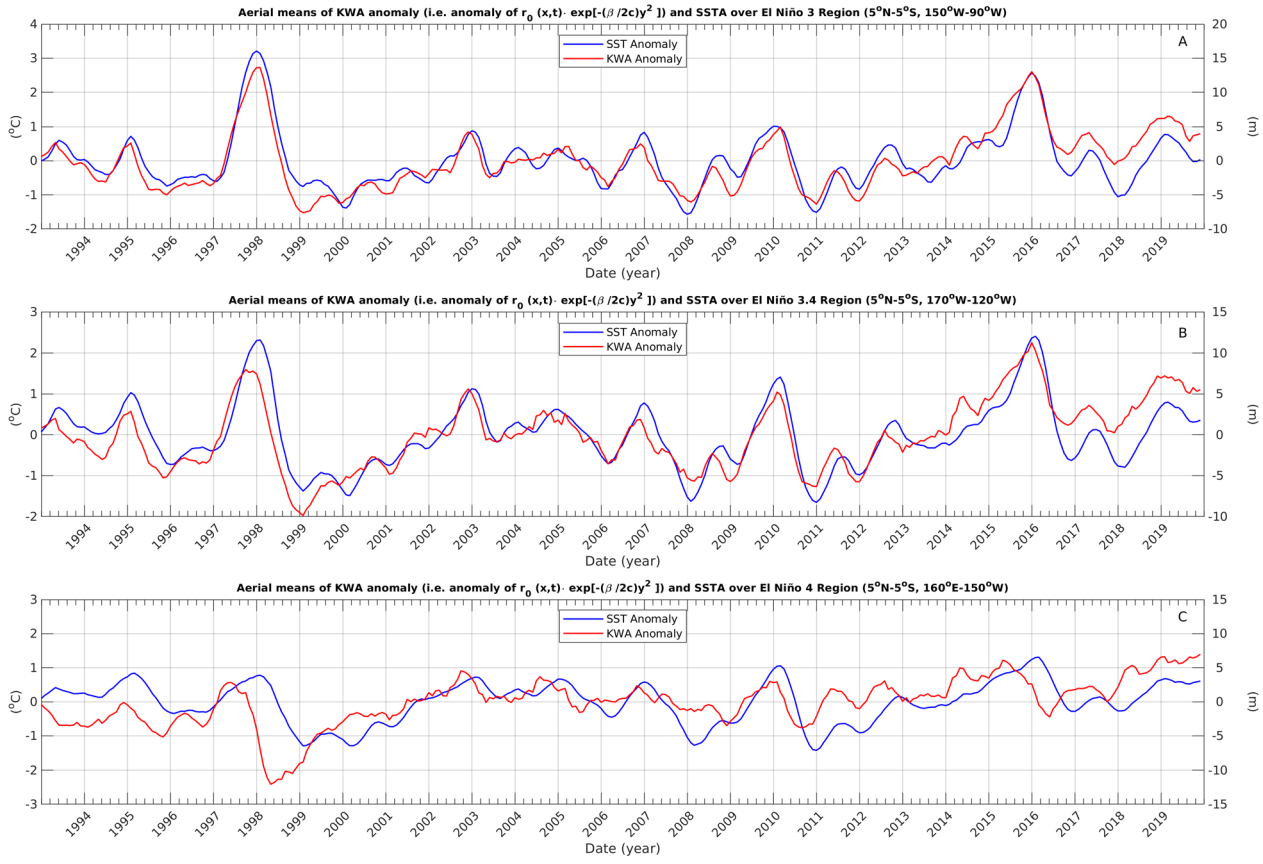

Figure 5. Aerial means of KW activity anomaly (defined as $\sigma_0(x,t)\cdot R_0(y\cdot(\beta/2c_1)^{1/2})$ with σ_0 the anomaly of the KW amplitude). Red line and aerial mean of the SSTA (blue line) over El Niño region 3 (**a**), 3.4 (**b**) and 4 (**c**).

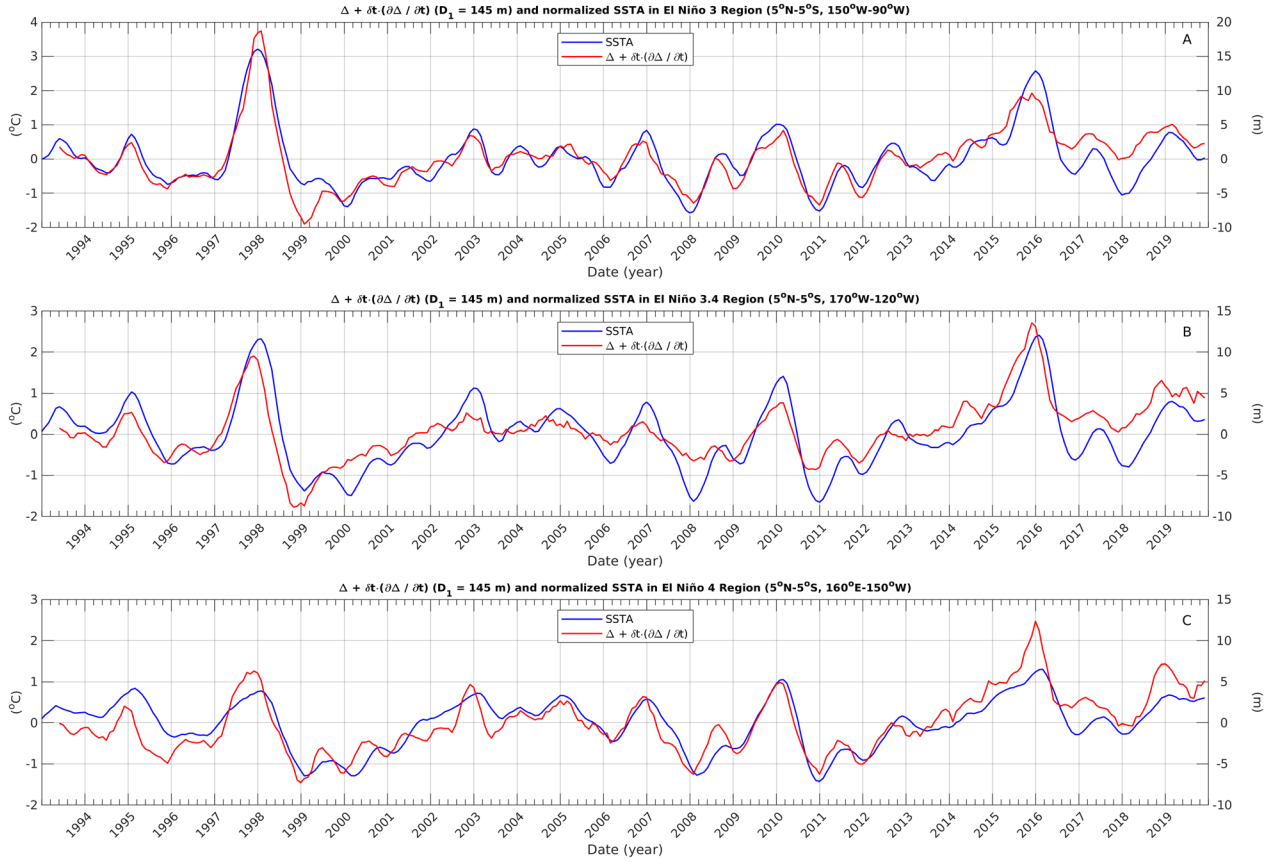

Figure 6. Aerial means of KW activity anomaly plus its time derivative (red line) and aerial mean of the SSTA (blue line, as in Figure 5 and reported just for the reader's convenience) over El Niño region 3 (**a**), 3.4 (**b**) and 4 (**c**).

4. Discussion

In this research, we studied internal KW propagation in relation to changes in the SSTA over the tropical Pacific. In situ and altimeter data have been used to discuss the propagation properties of KWs in relation to the stratification regime of the ocean. Assuming the ocean as a two-layer system, to interpret the relationships between changes in the SST and KW propagation, we developed an analytical model for KW propagation over a sloping pycnocline, named SIM, in which the slope of the pycncocline is sustained by constant zonal wind stress. Interestingly, KW propagation over a sloping pycncocline is different with respect to that over a flat interface, owing to the fact that the sloping interface produces a damping term in the wave equation. When variations in the pycnocline depth associated with propagating KWs are averaged over El Niño 3, 3.4 and 4 regions, this model leads to a Recharge/Discharge-like model. In this logic, our model can appear, at first sight, conceptually different from the Recharge/Discharge because, in the Recharge/Discharge, the equilibrium between the SSTA and changes in the depth of the pycnocline, is achieved by the collective action of Kelvin and Rossby waves.

Here, it has been assumed that only changes in the pycnocline depth associated with transiting KWs contribute to changes in the SSTA. However, we have also seen that changes in the average SSTA over El Niño regions 3, 3.4 and 4, can be reproduced accurately from changes in the pycnocline depth associated with transiting KWs using the SIM, which indicates that the primary factor determining changes in the SSTA are KWs, while RWs have a negligible effect. Following Eusebi Borzelli and Carniel [20], a possible explanation for this phenomenon could be related to the different propagation properties of KWs and RWs and the concept of potential vorticity conservation. We have seen that the pycncoline in

the tropical Pacific, west of the dateline, is nearly flat and starts sloping east of it (**Figure 3a**). Over a flat interface, KWs and RWs interact destructively and do not determine changes in the thermocline depth [19]. East of the dateline, where the pycncoline starts lowering, RWs propagating along the equator, to conserve potential vorticity, deviate poleward and leave the equatorial belt [21]. Conversely, when propagating over a sloping pycnocline, KWs cannot deviate poleward since, by definition, they are constrained to propagate zonally. So, east of the dateline RWs and KWs stop interacting and, in this region, KWs are left modifying efficiently the depth of the thermocline.

From the perspective discussed above, our data, along with the SIM, are consistent with the Recharge/Discharge paradigm. This demonstrates that the Recharge/Discharge model [7,8,22], in addition to being an elegant conceptual description of the ENSO cycle, can also be considered an important quantitative tool. This tool is based on a robust dynamic/thermodynamic background and can accurately represent the relationships between changes in the SSTA and vertical oscillations of the pycnocline depth, provided that it is recognized the predominant role of KWs in determining these oscillations.

Another interesting mechanism that we have documented here consists in KW damping. Altimeter data shows that KWs are regularly formed at the western boundary of the Pacific, but these waves, never travel a distance greater than, approximately, 5000 km and are damped before reaching the dateline. On the other hand, KWs formed near the dateline, in a region roughly between 170°E and 170°W, can travel freely for 11000 km and reach the eastern boundary of the basin. In this region, KWs are occasionally generated, but every time they are formed, an El Niño event is recorded. Furthermore, the further east the waves are generated, the more severe the El Niño event is classified. In our SIM, we have observed that a zonal wind with a mean intensity of 3.2 m/s results in an e-folding distance for KWs on the order of 90000 km. This distance is too long to explain the damping of KWs in the western Pacific.

To justify a damping distance as short as 5000 km, we would need to require a wind stress of 0.3 N/m^2 which implies an average zonal wind intensity of, approximately, 12–13 m/s, which is an unreasonable value. To explain this discrepancy, it can be speculated that other factors, besides the sloping pycnocline, are active to damp KWs in the western Pacific (i.e., west of, approximately, 170°E).

As previously discussed to explain that KWs are the primary factor determining changes in the SSTA with RWs playing a minor role, the first hypothesis to explain the damping of KWs in the western tropical Pacific, could be to relate it to the mutual annihilation of KWs and RWs propagating over a flat interface.

Another possible hypothesis is that internal waves, when transiting in a region symmetric with respect to the equator, cause an imbalance between wind stress and the shape of the pycnocline within that region. This imbalance is due to the time it takes for the wave to travel across the region, the time necessary for the pycnocline to return to its equilibrium position, and the time for the SSTA to react to changes in the depth of the pycncoline. To account for this delay, Burger and Jin [22] introduced a relaxation time for the fluctuation of the thermocline around its climatological state. Similarly, Zebiak and Cane [28] considered a damping term of the form -rσ in the continuity equation to describe the dynamic of the Intertropical Convergence Zones.

Burger and Jin [22] found a relaxation time of the eastern Pacific thermocline depth, caused by an initial perturbation originated in the western part of the basin, of 2 months (with reference to Burger and Jin [22], see ε_2 in equation 3). This value is close to the time necessary for a perturbation, propagating at a velocity of 2.2–2.3 m/s, to travel across the entire Pacific Ocean (i.e., from 130°E to 90°W ≈ $1.5 \cdot 10^4$ km, which implies approximately 78 days). In our case, KWs would take approximately 25 days to travel from 130°E to 170°E (≈ 5000 km). This suggests that KWs damping in the western Pacific may be due to the combined effect of the sloping pycncoline and the time necessary for the wave to travel between 130°E

and 170°E.

Another possible explanation for the disappearance of KWs in the western tropical Pacific around 170°E of KWs is that, near 170°E, the Inter-Tropical Convergence Zone and the South Pacific Convergence Zone merge [29]. In this region, zonal winds switch from the westerlies to the easterlies and the atmospheric environment changes from neutral to suppressing [30,31]. Wind stress components deduced from ERA5 data, averaged over the period Jan 1993–Aug 2019, shown in **Figures 7a and 7b**, actually demonstrate that, near by 170°E, the effect of the wind over the ocean surface is suppressing (i.e., the horizontal divergence of the wind stress is negative) thus providing an additional clue for a mechanism underlying wave blocking in this region.

Another interesting issue, confirming that KW damping is more effective between 130°E and 170°E than in the rest of the tropical Pacific, is that in El Niño region 4 (western Pacific), in order to reproduce changes in the SSTA from changes in the pycnocline depth, it is necessary to account for, differently from El Niño regions 3 (eastern Pacific) and 3.4 (central Pacific), the effect of the variation in the pycncolcine depth (i.e., $\partial\Delta/\partial t$). This means that, in El Niño regions 3 and 3.4, $\partial\Delta/\partial t \approx 0$, while, in El Niño region 4, $\partial\Delta/\partial t \neq 0$. This effect is related to wave damping, which is more effective in El Niño region 4 than in regions 3 and 3.4. Indeed, Equation (8) of Appendix, states that changes in aerial means around the equator of the pycnocline depth, depend upon differences in KW amplitudes at the zonal boundaries of the regions. Transiting in El Niño region 4, KWs are dumped more efficiently than in regions 3 and 3.4, with the result that, in El Niño region 4, values of $\partial\Delta/\partial t$ are appreciably different from zero.

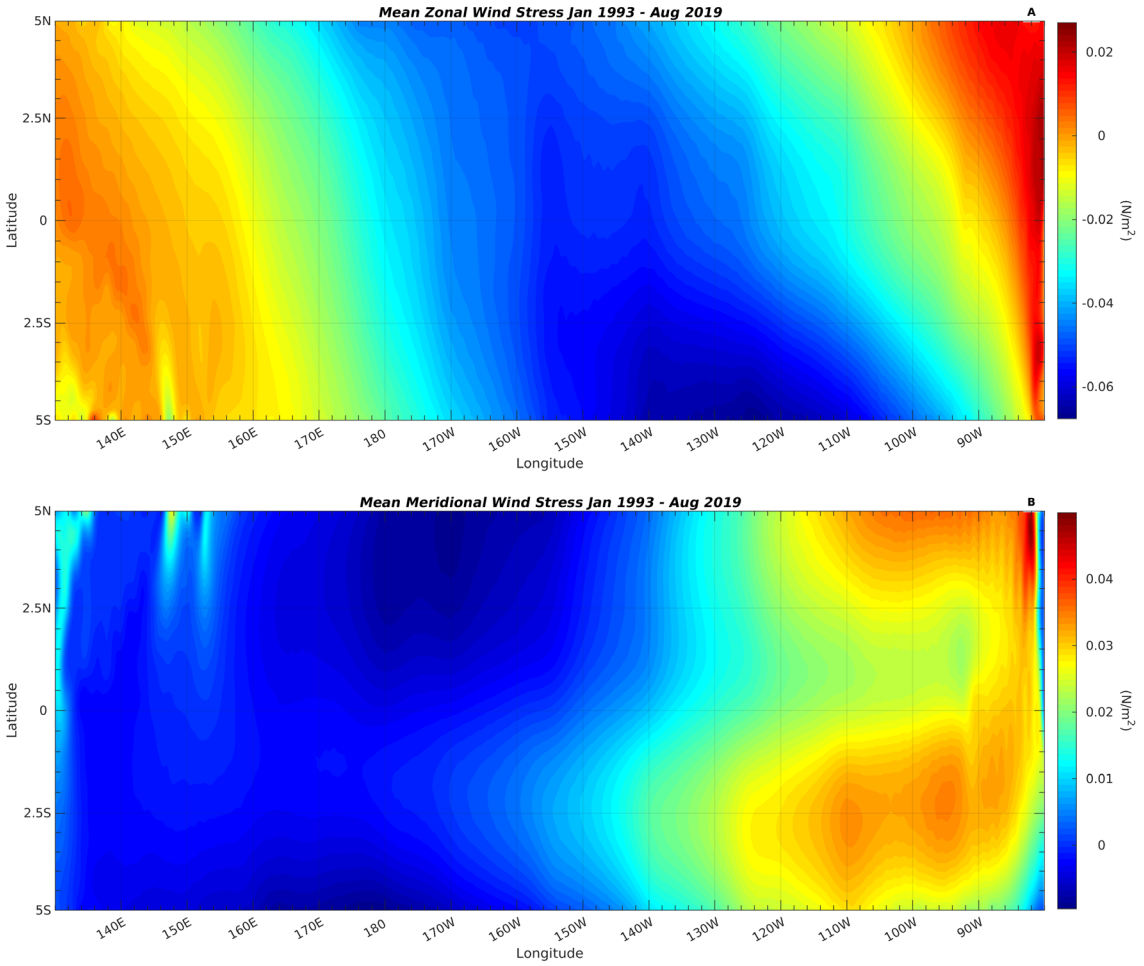

Figure 7. Mean zonal (**a**) and meridional (**b**) wind stress over the period Jan 1993–Aug 2019.

5. Conclusions

In this research, we have discussed the propagation of Kelvin waves concerning changes in the sea surface temperature anomaly. Our findings show a strong correlation between changes in the sea surface temperature anomaly in the El Niño 3, 3.4 and 4 regions and the passage of Kelvin waves. To further understand this relationship, we have developed a new analytical model, the Sloping Interface Model, which relates Kelvin wave propagation over a sloping interface to changes in the sea surface temperature anomaly.

Our research also highlights the importance of Kelvin wave damping, which occurs when the wave travels over a sloping interface, in triggering variations in the sea surface temperature anomaly in El Niño regions 3, 3.4 and 4. However, we have also observed that Kelvin waves formed at the western boundary of the Pacific Ocean experience damping before reaching the dateline, resulting in no recorded El Niño event. On the other hand, Kelvin waves that form nearer to the dateline propagate freely for approximately 11,000 kilometers and reach the eastern boundary of the basin with little to no significant damping. To explain this phenomenon, we have proposed a mechanism involving the mutual annihilation of Kevin and Rossby waves propagating over a flat interface.

Our research primarily focuses on the initiation of El Niño. However, the strong correlation between changes in sea surface temperature anomalies in the Niño regions and displacements of the main pycncoline due to the passage of Kelvin waves, suggests that Kelvin waves also play a key role in the onset of La Niña. It is important to note that the propagation of Kelvin waves during La Niña differs from that during El Niño. While El Niño events are accompanied by Kelvin waves generated in the central Pacific, during La Niña, Kelvin waves emerge from the western Pacific coast, travel freely through the entire tropical Pacific Ocean, and reach the eastern boundary of the basin. We have named this different behavior of Kelvin waves about El Niño and La Niña as an "asymmetry". This "asymmetry" is an interesting issue that warrants further investigation and dedicated research.

Several questions remain open at this point, first to simplify the formalism, in the Sloping Interface Model, we have considered Kelvin wave propagation with a constant velocity and the sloping pycnocline, summarizing the background climatological state, has been considered only as a damping wave factor. We have, however, seen that the velocity of the first baroclinic mode, displays remarkable variations along the zonal direction, which are expected to affect Kelvin wave propagation. It is therefore our intent, to provide more rigorous analytical arguments, which are able to account for spatial changes in the velocity of the first baroclinic mode in relation to Kelvin wave propagation.

As a final remark, we believe that the results presented here make an important contribution to our understanding of the relationships between variations in sea surface temperature anomalies and the propagation of internal waves in the tropical Pacific.

Author Contributions

G.L.E.B and A.S. contributed equally to the work, by proposing the original idea and designing the research. G.L.E.B. verified the analytical methods. Both authors analyzed the data and provided the figures and table. Both authors contributed to interpreting the results. G.L.E.B. wrote the initial version of the manuscript and A.S. provided corrections and comments.

Conflicts of Interest

The authors declare no conflict of interest.

Data Availability Statement

Altimeter and T-S data can be respectively downloaded from Copernicus Marine Service at:

https://resources.marine.copernicus.eu/product-detail/SEALEVEL_GLO_PHY_L4_MY_008_047/INFORMATION

https://resources.marine.copernicus.eu/prod-

uct-detail/MULTIOBS_GLO_PHY_TSUV_3D_MYNRT_015_012/INFORMATION

Wind data are monthly means of the ERA-Interim project (prod. #627.1, doi: 10.5065/D68050NT) downloaded from:

https://rda.ucar.edu/datasets/ds627.1/#!access

Sea surface temperature data have been dowloaded from the Met Office Hadley Centre at:

https://www.metoffice.gov.uk/hadobs/hadisst/

Funding

This research received no external funding.

Acknowledgments

Altimeter and T-S data were provided by the Marine Service of the Copernicus Program-Europe's Eyes on Earth of the European Union. Wind data were obtained from the Research Data Archive managed by the Data Engineering and Curation Section of the Computational and Information Systems Laboratory at the National Center for Atmospheric Research (NCAR) in Boulder, Colorado, USA. Sea Surface Temperature data were downloaded from the Met Office Hadley Centre. Copernicus, NCAR and Met Office staff are greatly acknowledged for maintaining and distributing these data sets.

References

[1] Bjerknes, J., 1969. Atmospheric teleconnections from the equatorial Pacific. Monthly Weather Review. 97(3), 163–172. DOI: https://doi.org/10.1175/1520-0493(1969)097<0163:ATFTEP>2.3.CO;2

[2] Wyrtki, K., 1975. El Niño—the dynamic response of the equatorial Pacific Oceanto atmospheric forcing. Journal of Physical Oceanography. 5(4), 572–584. DOI: https://doi.org/10.1175/1520-0485(1975)005<0572:ENTDRO>2.0.CO;2

[3] Rasmusson, E.M., Wang, X., Ropelewski, C.F., 1990. The biennial component of ENSO variability. Journal of Marine Systems. 1(1–2), 71–96. DOI: https://doi.org/10.1016/0924-7963(90)90153-2

[4] Jiang, N., Neelin, J.D., Ghil, M., 1995. Quasi-quadrennial and quasi-biennial variability in the equatorial Pacific. Climate Dynamics. 12, 101–112. DOI: https://doi.org/10.1007/BF00223723

[5] Torrence, C., Compo, G.P., 1998. A practical guide to wavelet analysis. Bulletin of the American Meteorological Society. 79(1), 61–78. DOI: https://doi.org/10.1175/1520-0477(1998)079<0061:APGTWA>2.0.CO;2

[6] Philander, S.G., 1990. El Nino, La Nina and the southern oscillation. Academic Press: New York.

[7] Jin, F.F., 1997. An equatorial ocean recharge paradigm for ENSO. Part I: Conceptual model. Journal of the Atmospheric Sciences. 54(7), 811–829. DOI: https://doi.org/10.1175/1520-0469(1997)054<0811:AEORPF>2.0.CO;2

[8] Jin, F.F., 1997. An equatorial ocean recharge paradigm for ENSO. Part II: A stripped-down coupled model. Journal of the Atmospheric Sciences. 54(7), 830–847. DOI: https://doi.org/10.1175/1520-0469(1997)054<0830:AEORPF>2.0.CO;2

[9] Chen, D., Cane, M.A., Kaplan, A., et al., 2004. Predictability of El Niño over the past 148 years. Nature. 428, 733–736. DOI: https://doi.org/10.1038/nature02439

[10] Chen, D., Cane, M.A., 2008. El Niño prediction and predictability. Journal of Computational Physics. 227(7), 3625–3640. DOI: https://doi.org/10.1016/j.jcp.2007.05.014

[11] Suarez, M.J., Schopf, P.S., 1988. A delayed action oscillator for ENSO. Journal of the Atmospheric Sciences. 45(21), 3283–3287. DOI: https://doi.org/10.1175/1520-0469(1988)045<3283:ADAOFE>2.0.CO;2

[12] Battisti, D.S., Hirst, A.C., 1989. Interannual variability in a tropical atmosphere-ocean model: Influence of the basic state, ocean geometry

and nonlinearity. Journal of the Atmospheric Sciences. 46(12), 1687–1712.
DOI: https://doi.org/10.1175/1520-0469(1989)046<1687:IVIATA>2.0.CO;2

[13] Picaut, J., Delcroix, T., 1995. Equatorial wave sequence associated with warm pool displacements during the 1986–1989 El Niño-La Niña. Journal of Geophysical Research. 100(C9), 18393–18408.
DOI: https://doi.org/10.1029/95JC01358

[14] Fedorov, A.V., Harper, S.L., Phiander, G., et al., 2003. How predictable is El Niño? Bulletin of the American Meteorological Society. 84(7), 911–920.
DOI: https://doi.org/10.1175/BAMS-84-7-911

[15] Arora, A., 2022. The effect of the variability of wind forcing on ENSO simulation in an OGCM: case of canonical and protracted event. Theoretical and Applied Climatology. 147, 265–281.
DOI: https://doi.org/10.1007/s00704-021-03816-5

[16] Arora, A., Kumar, S., 2019. What makes protracted El Niño to last longer than canonical El Niño? Theoretical and Applied Climatology. 136, 587–603.
DOI: https://doi.org/10.1007/s00704-018-2503-8

[17] Wang, C., Fiedler, P.C., 2006. ENSO variability and the eastern tropical pacific: A review. Progress in Oceanography. 69(2–4), 239–266.
DOI: https://doi.org/10.1016/j.pocean.2006.03.004

[18] Santoso, A., Mcphaden, M.J., Cai, W. 2017. The defining characteristics of ENSO extremes and the strong 2015/2016 El Niño. Reviews of Geophysics. 55(4), 1079–1129.
DOI: https://doi.org/10.1002/2017RG000560

[19] Kang, I.S., An, S.I., 1998. Kelvin and Rossby wave contributions to the SST oscillation of ENSO. Journal of Climate. 11(9), 2461–2469.
DOI: https://doi.org/10.1175/1520-0442(1998)011<2461:KARWCT>2.0.CO;2

[20] Eusebi Borzelli, G.L., Carniel, S., 2023. Where the winds clash: What is really triggering El Niño initiation?. npj Climate and Atmospheric Science. 6, 119.
DOI: https://doi.org/10.1038/s41612-023-00445-9

[21] Yang, J., Yu, L., 1992. Propagation of equatorially trapped waves on a sloping thermocline. Journal of Physical Oceanography. 22(6), 573–582.
DOI: https://doi.org/10.1175/1520-0485(1992)022<0573: POETWO>2.0.CO;2

[22] Burger, G., Jin, F.F., 2005. The simplest ENSO recharge oscillator. Geophysical Research Letters. 32(13).
DOI: https://doi.org/10.1029/2005GL022951

[23] Boulanger, J.P., Menkes, C., 1995. Propagation and reflection of long equatorial waves in the Pacific Ocean during the 1992–1993 El Nino. Journal of Geophysical Research. 100(C12), 25041–25059.
DOI: https://doi.org/10.1029/95JC02956

[24] Boulanger, J.P., Menkes, C., 1999. Long equatorial wave reflection in the Pacific Ocean from TOPEX/POSEIDON data during the 1992–1998 period. Climate Dynamics. 15, 205–225.
DOI: https://doi.org/10.1007/s003820050277

[25] Boulanger, J.P., Cravatte, S., Menkes, C., 2003. Reflected and locally wind-forced interannual equatorial Kelvin waves in the western Pacific Ocean. Journal of Geophysical Research. 108(C10).
DOI: https://doi.org/10.1029/2002JC001760

[26] Gill, A.E., 1982. Atmosphere-ocean dynamics. Academic Press: Cambridge.

[27] Fidler, P.C., Mendelssohn, R., Palacios, D.M., et al., 2013. Pycnocline variations in the eastern tropical and north pacific, 1958–2008. Journal of Climate. 26(2), 583–599.
DOI: https://doi.org/10.1175/JCLI-D-11-00728.1

[28] Zebiak, S.E., Cane, M.A., 1987. A model El Niño–Southern oscillation. Monthly Weather Review. 115(10), 2262–2278.
DOI: https://doi.org/10.1175/1520-0493(1987)115<2262:AMENO>2.0.CO;2

[29] Jaffrés, J.B.D., Cuff, C., Rasmussen, C., et

al., 2018. Teleconnection of atmospheric and oceanic climate anomalies with Australian weather patterns: A review of data availability. Earth-Science Reviews. 176, 117–146.
DOI: https://doi.org/10.1016/j.earscirev.2017.08.010

[30] Zhang, C., 2015. Climate and climate change | Global impacts of the Madden-Julian oscillation. Encyclopedia of atmospheric sciences (second edition). Academic Press: Cambridge. pp. 73–79.
DOI: https://doi.org/10.1016/B978-0-12-382225-3.00510-7

[31] Sullivan, A., Zhong, W., Eusebi Borzelli, G.L., et al., 2021. Generation of westerly wind bursts by forcing outside the tropics. Scientific Reports. 11, 912.
DOI: https://doi.org/10.1038/s41598-020-79655-7

[32] Wunsch, C., 1998. The work done by the wind on the oceanic general circulation. Journal of Physical Oceanography. 28(11), 2332–2340.
DOI: https://doi.org/10.1175/1520-0485(1998)028<2332:TWDBTW>2.0.CO;2

Appendix

The sloping interface model

Here we derive the SIM model equations based on the two layers ocean shallow water theory and show the relationships with Jin's Recharge/Discharge model [7,8,22].

Dynamics

We assume that the tropical Pacific can be described as a two-layer system over a flat bottom, with the surface and bottom densities equal to ρ_1 and ρ_2. We also assume that, in a given bounded region S, symmetric respect to the equator (typically ENSO region 3 or 3.4 or 4), the surface and bottom layers are at the hydrostatic equilibrium and the surfaces are kept in shape by constant easterly wind stress $\tau=(\tau_x,0)$ (i.e., perfect Svedrup balance between wind stress and the sea surface deformation). In this situation, we have that the surface and interface layers are $\eta = \eta_{eq}$ and $h = h_{eq}$, and the thickness of the surface and bottom layer are $H_1 = H_1^{(eq)} = D_1 + \eta_{eq} - h_{eq}$ and $H_2 = = H_2^{(eq)} = D_2 + h_{eq}$. Hydrostatic equilibrium provides a relationship between the wind stress and the shape of surface and bottom layers, namely $\partial\eta_{eq}/\partial x = \tau_x/(gH_1\rho_1) \approx \tau_x/(gD_1\rho_1)$, $\partial\eta_{eq}/\partial y = 0$, $\partial h_{eq}/\partial x \approx -\tau_x/(g'D_1\rho_2)$ and $\partial h_{eq}/\partial y = 0$ (i.e., $\partial\eta_{eq}/\partial x - \partial h_{eq}/\partial x) \approx \tau_x/(g'D_1\rho_1)$). Suppose, now, that a small disturbance $p(x,y,t)$, which does not induce meridional transport (i.e., $v_1 = v_2 = 0$, where $v_{1\text{-}2}$ refers to the meridional velocity in the surface and bottom layer) propagates eastward over the sloping interface layer, leaving the signature $\sigma(x,y,t)$ over the surface layer. We have:

$$H_1 = D_1 + \eta_{eq} - h_{eq} + \sigma - p$$

$$H_2 = D_2 + h_{eq} + p$$

and the equation of motion for u_1, u_2, σ and p are the two layers of shallow water equations over the equatorial β-plane, i.e.,

$$\frac{\partial u_1}{\partial t} = -g\frac{\partial \sigma}{\partial x} \tag{1a}$$

$$\beta y u_1 = -g\frac{\partial \sigma}{\partial y} \tag{1b}$$

$$\frac{\partial H_1}{\partial t} + \frac{\partial\left(H_1 \cdot u_1\right)}{\partial x} = 0 \tag{1c}$$

$$\frac{\partial u_2}{\partial t} = -g\frac{\rho_1}{\rho_2}\frac{\partial \sigma}{\partial x} - g'\frac{\partial p}{\partial x} \tag{1d}$$

$$\beta y u_2 = -g\frac{\rho_1}{\rho_2}\frac{\partial \sigma}{\partial y} - g'\frac{\partial p}{\partial y} \tag{1e}$$

$$\frac{\partial H_2}{\partial t} + \frac{\partial\left(H_2 \cdot u_2\right)}{\partial x} = 0 \tag{1f}$$

Note that, in this idealized model, the anomaly of the pycnocline depth is exactly σ-p (i.e., $H_1^{(anomaly)} = H_1\text{-}H_1^{(eq)}$). Our objective is to derive, as in Jin's model [7,8,22], a dynamical equation for the aerial average of the pycncocline depth anomaly, which we define as:

$$\Delta = \frac{1}{L_x \cdot L_y}\iint_{(S)} dxdy \cdot \left(H_1 - H_1^{(eq)}\right) = \frac{1}{L_x \cdot L_y}\iint_{(S)} dxdy \cdot \left(\sigma - p\right)$$

where L_x and L_y are the zonal and meridional length of S. Integrating Equation (1c) over S, we get:

$$\frac{\partial \Delta}{\partial t} + \frac{1}{L_x \cdot L_y}\iint_{(S)} dxdy \frac{\partial\left[u_1 \cdot \left(D_1 + \eta_{eq} - h_{eq} + \sigma - p\right)\right]}{\partial x} \approx$$

$$\approx \frac{\partial \Delta}{\partial t} + \frac{1}{L_x \cdot L_y}\iint_{(S)} dxdy \frac{\partial\left[u_1 \cdot \left(D_1 + \frac{\tau_x \cdot x}{g' D_1 \rho_1}\right)\right]}{\partial x} = 0$$

where the last step is justified by linearization and the fact that $\eta_{eq} - h_{eq} = \tau_x \cdot x / (\rho_1 \cdot D_1 \cdot g')$. Integrating over the zonal direction and assuming $\rho_1 = const.$ we get:

$$\frac{\partial \Delta}{\partial t} + \frac{D_1}{L_x \cdot L_y}\int_{y_1}^{y_2} dy\left[u_1(x_2,y,t) - u_1(x_1,y,t)\right] +$$

$$+ \frac{\tau_x}{g' \cdot D_1 \cdot \rho_1 \cdot L_x \cdot L_y}\int_{y_1}^{y_2} dy\left[x_2 \cdot u_1(x_2,y,t) - x_1 \cdot u_1(x_1,y,t)\right] = 0 \tag{2}$$

Without making a specific hypothesis on the algebraic structure of the solutions to the system (1), it is difficult to get further information on the integrals in (2). To proceed, here, we seek solutions to (1) of the form $p(x,y,t) = \mu(x)\sigma(x,y,t)$ and set $\mu(x)$ in order to have a propagation speed that, in the limit $\tau_x \to 0$, converges to the propagation speed of a KW over a flat interface.

After what is stated above, putting $p(x,y,t) = \mu(x)\sigma(x,y,t)$ in (1c), differentiating (1c) with respect to t and (1a) with respect to x we get an equation for the sea surface deformation.

$$\frac{\partial^2\sigma}{\partial t^2} - c_1^2(x)\cdot\frac{\partial^2\sigma}{\partial x^2} - \left(\frac{\tau_x}{D_1\rho_1}\right)\cdot\frac{\partial\sigma}{\partial x} = 0 \tag{3}$$

where we have set:

$$1-\mu(x) = \left(\frac{g}{g'}\right)\cdot\frac{D_1 + D_2 + \eta_{eq}(x)}{D_2 + h_{eq}(x)} \approx \frac{g}{g'} \tag{4}$$

$$c_1(x) = \sqrt{g'\cdot[D_1 + \eta_{eq}(x) - h_{eq}(x)]} \tag{5}$$

In the following, we shall always assume the $1\text{-}\mu = g/g'$, which implies the form (5) for the velocity of the internal wave. With a similar procedure, differentiating (1c) with respect to x and (1a) with respect to t, after putting $p(x,y,t) = \mu\sigma(x,y,t)$ in (1c), we get for the velocity field:

$$\frac{\partial^2 u_1}{\partial t^2} - c_1^2(x)\cdot\frac{\partial^2 u_1}{\partial x^2} - \left(\frac{\tau_x}{D_1\cdot\rho_1}\right)\cdot\frac{\partial u_1}{\partial x} = 0 \tag{6}$$

At this point, it could be possible to continue analytically by showing that both Equations (3) and (6) have separate variable solutions and that, in both cases, the zonal parts of σ and u_1 satisfy a Sturm-Liouville eigenvalue problem with damping coefficient $\gamma = [\tau_x/(D_1\rho_1)]$, but we believe that such long analytical treatment is far beyond the scopes of this presentation. Here, to keep the formalism as simple as possible, it suffices to say that, if the equilibrium deformations of the free and interface layers are small for the depth of the surface layer (i.e., $D_1 \gg \eta_{eq} - h_{eq}$), c_1 becomes the velocity of a KW propagating over a flat interface of depth D_1 (i.e., $c_1 \approx (g'D_1)^{1/2}$) and that the solution to (3) satisfying (1b) and boundary conditions at the poles $\sigma \to 0$ as $y \to \pm\infty$ is:

$$\sigma(x,y,t) = r_0(x,t)\cdot e^{-\frac{\beta}{2\cdot c_1}\cdot y^2} \tag{7a}$$

and, similarly

$$u_1(x,y,t) = \left(\frac{g}{c_1}\right)\sigma(x,y,t) = \left(\frac{g}{c_1}\right)\cdot r_0(x,t)\cdot e^{-\frac{\beta}{2\cdot c_1}\cdot y^2} \tag{7b}$$

where $r_0(x,t)$ represents a spatially damped oscillation with a damping rate of the form $exp[-x\cdot\gamma/(2c_1^2)]$. In order to make the treatment more concise, it is at this point important to review an elementary formula [22] to relate the average depth of the thermocline over the entire tropical Pacific with the thermocline depth in the western and eastern Pacific (i.e., $h \approx 0.5\cdot(h_w + h_e)$), which relates the average value of a function in an interval with the values of the function at the boundaries of the interval, i.e.,

$$\langle f \rangle = \int_{x_1}^{x_2}\frac{f(x)}{x_2 - x_1}dx \approx \frac{1}{2}\frac{f(x_2) - f(x_1)}{x_2 - x_1}(x_1 + x_2) \tag{8}$$

which can be obtained by setting $f(x) \approx a\cdot x + b$ with $a = (f(x_2) - f(x_1))/(x_2 - x_1)$ and the coordinate system has been chosen in order to have $b = 0$.

With this material at hand, we are now in the position to estimate the integrals in Equation (2). Indeed, by substituting (7b) into the first integral in (2) and using (8), we get

$$\begin{aligned}
&\frac{D_1}{L_x\cdot L_y}\int_{y_1}^{y_2} dy[u_1(x_2,y,t) - u_1(x_1,y,t)] = \\
&= \frac{D_1\cdot g}{c_1\cdot L_x\cdot L_y}\cdot\int_{y_1}^{y_2} dy[\sigma(x_2,y,t) - \sigma(x_1,y,t)] \approx \\
&\approx \frac{2gD_1}{c_1\cdot(x_1 + x_2)\cdot L_x\cdot L_y}\int_{x_1}^{x_2}\int_{y_1}^{y_2} dxdy\sigma(x,y,t) = \\
&= \frac{2g\cdot D_1}{c_1\cdot(x_1 + x_2)}\cdot\frac{1}{1-\mu}\cdot\Delta = \frac{2g'\cdot D_1}{c_1\cdot(x_1 + x_2)}\cdot\Delta
\end{aligned} \tag{9a}$$

The second integral in Equation (2) is more difficult, but it can be estimated by observing that it is related to the work done by the background wind over the propagating KW. Indeed, the work per unit time exerted by the background wind over the perturbation current [32] is $W \approx u_1(x,y,t)\cdot\tau_x/[\rho_1 H_1^{(eq)}(x)] \approx [u_1(x,y,t)\cdot\tau_x/(\rho_1 D_1)]\cdot[1-x\cdot\tau_x/(g' D_1\rho_1)]$, so that:

$$\frac{\tau_x}{g' D_1\rho_1 L_x\cdot L_y}\int_{y_1}^{y_2} dy\left[x_2\cdot u_1(x_2,y,t)-x_1\cdot u_1(x_1,y,t)\right]\approx$$
$$\approx D_1^2\cdot\rho_1\frac{\langle W(x_1,y,t)\rangle_y-\langle W(x_2,y,t)\rangle_y}{L_x}+$$
$$-D_1\cdot\tau_x\cdot\frac{\langle u_1(x_1,y,t)\rangle_y-\langle u_1(x_2,y,t)\rangle_y}{L_x}\approx$$
$$\approx -2D_1^2\cdot\rho_1\cdot\frac{\langle W\rangle}{x_1+x_2}+2D_1\cdot\tau_x\cdot\frac{\langle u_1\rangle}{x_1+x_2}=2D_1^2\cdot\frac{\langle u_1/D_1-u_1/H_1\rangle}{x_1+x_2}\cdot\tau_x \tag{9b}$$

where the symbol <> indicates averaging over the region S and the symbol $<>_y$ indicates averaging along the meridional direction. Substituting (9a) and (9b) into Equation (2), we get:

$$\frac{\partial\Delta}{\partial t}+\frac{2g'\cdot D_1}{c_1\cdot(x_1+x_2)}\cdot\Delta+$$
$$+2D_1^2\cdot\frac{\langle u_1/D_1-u_1/H_1\rangle}{x_1+x_2}\cdot\tau_x=0 \tag{10}$$

which is formally similar to the prognostic equation for the variability in the aerial average of the pycnocline depth found by Burger and Jin [22].

Thermodynamics

As in the section devoted to the dynamics, we consider the ocean as a two layered system of constant density (i.e., constant temperature and salinity), initially at the hydrostatic equilibrium, where the surface and interface layers are kept in shape by constant zonal wind stress. The average temperature over the water column, at the equilibrium state which is:

$$T^{(eq)}=\frac{T_1\cdot(D_1+\eta_{eq}-h_{eq})+T_2\cdot(D_2+h_{eq})}{D_1+D_2+\eta_{eq}}\approx$$
$$\approx\frac{T_1\cdot(D_1+\eta_{eq}-h_{eq})+T_2\cdot(D_2+h_{eq})}{D_1+D_2} \tag{11}$$

Note that, the zonal wind stress produces a zonal gradient in the depth averaged temperature. We want to study the temperature fluctuation around the equilibrium temperature (i.e., the temperature anomaly) induced by propagating KWs. Obviously, indicating with θ the temperature anomaly, we have:

$$\theta\approx\frac{T_1\cdot(\sigma-p)+T_2\cdot p}{D_1+D_2}=\frac{T_1\cdot(1-\mu)\sigma+T_2\cdot\mu\sigma}{D_1+D_2}\approx$$
$$\approx\frac{g}{g'}\cdot\frac{T_2-T_1}{D_1+D_2}\cdot\sigma=A_{\theta\sigma}\sigma \tag{12}$$

where, in the last step, the term T_2 has been neglected with respect to $T_2\cdot(g/g')$ and shows that, in our model, changes in the temperature anomaly and changes in the pycncoline depth anomaly are proportional. This implies that provided that coefficients of Equation (10) are scaled by $A_{\theta\sigma}/(1-\mu) = g'A_{\theta\sigma}/g$, the aerial averaged temperature anomaly obeys Equation (10) too, which describes the time variability in an aerial mean of pycnocline depth anomaly.